Magnetic Alignment of Block Copolymer Microdomains by Intrinsic Chain Anisotropy

Yekaterina Rokhlenko, Manesh Gopinadhan, Chinedum O. Osuji, Kai Zhang, Corey S. O'Hern, Steven R. Larson, Padma Gopalan, Paweł W. Majewski, and Kevin G. Yager

Phys. Rev. Lett. **115**, 258302 — Published 18 December 2015

DOI: 10.1103/PhysRevLett.115.258302

Magnetic alignment of block copolymer microdomains by intrinsic chain anisotropy

Yekaterina Rokhlenko, Manesh Gopinadhan, and Chinedum O. Osuji

Department of Chemical Engineering, Yale University, New Haven CT 06511

Kai Zhang and Corey S. O'Hern

Department of Mechanical Engineering and Materials Science, Yale University, New Haven CT 06511

Steven R. Larson and Padma Gopalan

Department of Materials Science and Engineering, University of Wisconsin, Madison WI 53706

Paweł W. Majewski and Kevin G. Yager

Center for Functional Nanomaterials, Brookhaven National Lab, Upton NY 11973

(Dated: December 14, 2015)

We examine the role of intrinsic chain susceptibility anisotropy in magnetic field directed self-assembly of a block copolymer using *in situ* X-ray scattering. Alignment of a lamellar mesophase is observed on cooling across the disorder-order transition with the resulting orientational order inversely proportional to the cooling rate. We discuss the origin of the susceptibility anisotropy, $\Delta\chi$, that drives alignment, and calculate its magnitude using coarse-grained molecular dynamics to sample conformations of surface-tethered chains, finding $\Delta\chi \approx 2 \times 10^{-8}$. From field-dependent scattering data we estimate grains of ≈ 1.2 μm are present during alignment. These results demonstrate that intrinsic anisotropy is sufficient to support strong field-induced mesophase alignment and suggest a versatile strategy for field control of orientational order in block copolymers.

PACS numbers: 82.35.Jk,82.35.Lr,81.16.Dn

Block copolymers (BCPs) self-assemble to form periodic structures on mesoscopic length scales. Such self-assembly is driven by phase separation of chemically distinct segments, with the extent of demixing limited by their physical connectivity. The characteristic length scales therefore are largely defined by the size, or molecular weight (MW), of the polymer chain. Considerable efforts have been devoted to developing methods to reliably direct BCP self-assembly, i.e. to align BCP domains, in various device- or application-relevant geometries and length scales [1, 2]. Electric fields have been used quite effectively in this regard [3–5].

Under appropriate circumstances, magnetic fields can also dictate the alignment of BCP mesophases in a highly efficacious manner [6]. Orientational order develops due to anisotropic field interactions that are sufficiently large to overcome thermal forces. The alignment response is a function of the anisotropy in magnetic susceptibility, $\Delta\chi = \chi_{\parallel} - \chi_{\perp}$, where the parallel direction is along the axis of highest rotational symmetry. The system free energy density, ϵ_m, is a function of the angle φ between the field and this parallel direction, and of the field strength, B, Eq. 1. For an ensemble of anisotropic objects, ϵ_m can be expressed in terms of the orientation distribution coefficient $\langle P_2(\cos\varphi)\rangle = \langle \frac{1}{2}(3\cos^2\varphi - 1)\rangle$, Eq. 2. The energy difference between orthogonal alignments is $\Delta\epsilon_m = -\Delta\chi B^2/2\mu_0$. Strong alignment occurs when this magnetostatic energy for structurally coherent units, grains, is significant compared to thermal motion, i.e., for $|\Delta E_m| = |\Delta\epsilon_m| V_g \gg k_B T$, where $V_g = \xi^3$ is the volume of a grain with dimension ξ. Alignment can therefore occur for suitably large grains, field strengths or magnetic susceptibility anisotropies.

$$\epsilon_m = \frac{-B^2}{2\mu_0}\left(\chi_{\parallel}\cos^2\varphi + \chi_{\perp}\sin^2\varphi\right) \tag{1}$$

$$\epsilon_m = \frac{-\Delta\chi B^2}{3\mu_0}\langle P_2(\cos\varphi)\rangle \tag{2}$$

Prior work has relied on liquid crystalline (LC) [7–10] or crystalline [11] assembly of rigid moities integrated with the BCP to achieve a sufficiently large $\Delta\chi$ for alignment at reasonable field strengths. Prototypical mesogenic units such as cyanobiphenyl species have $\Delta\chi \approx 10^{-6}$ (in SI dimensionless volume units) [12, 13]. $\Delta\chi$ is very small for typical BCPs in the absence of mesogenic groups. Shape anisotropy notwithstanding, for a lamellar diblock copolymer with volume fractions ϕ_A and ϕ_B, the anisotropy, with respect to the lamellar normal, is $\Delta\chi = -(\chi_A - \chi_B)^2/[(\chi_A/\phi_A) + (\chi_B/\phi_B)]$ where χ_A and χ_B are isotropic block susceptibilities. On this basis, for a typical symmetric non-LC BCP such as poly(styrene-b-4-vinylpyridine), $\Delta\chi \sim \mathcal{O}(10^{-10})$ [14, 15]. This results in

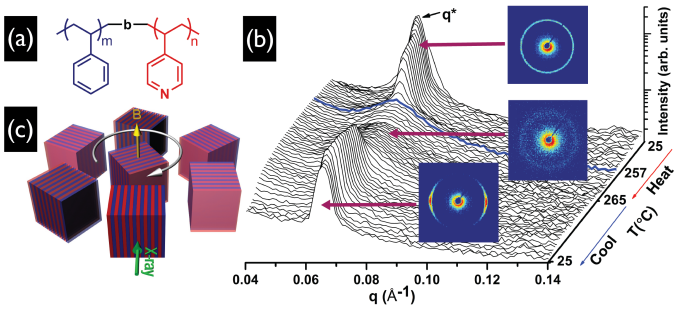

FIG. 1. (a) Chemical structure of PS-b-P4VP. (b) Temperature resolved SAXS data (25 → 265 → 25 °C) under 6 T field applied vertically. 2-D diffractograms are shown inset at three representative temperatures. T_{odt}=257 °C, d-spacing=9.5 nm. (c) Schematic illustrating degenerate system alignment with lamellar normals perpendicular to the field.

a significantly smaller driving force for alignment, and as a result magnetic field alignment of such 'coil-coil' BCPs has not been observed to date.

Here, we describe *in situ* X-ray scattering experiments of a coil-coil BCP subjected to high magnetic fields. Cooling across the disorder-order transition under the field induces alignment of the lamellar normals perpendicular to the field, suggesting the presence of $\Delta\chi$ of a non-trivial magnitude. The existence of such anisotropy is rationalized in terms of the intrinsic anisotropy of individual Gaussian chains and the non-zero ensemble average of such anisotropies due to the organization of the chain junctions along the lamellar interface between the blocks. We use molecular dynamics (MD) to estimate the intrinsic anisotropy of the system by simulating trajectories of representative chains.

The system is poly(styrene-b-4-vinyl pyridine) (PS-b-P4VP), Fig.1a, of MW 5.5 kg/mol (K) and PS weight fraction, f_{PS}=0.49, obtained from Polymer Source. Data presented here are for this 5.5K material. A well-purified secondary sample (MW=5.2K and f_{PS}=0.50) was prepared by living anionic polymerization for verification purposes. SAXS was conducted as samples were cooled (0.1 to 2 °C/min) across the order-disorder transition (ODT), under fields from 0 to 6 T. Further details are available in the Supplemental Material [16].

Temperature resolved SAXS data during heating and subsequent cooling at 0.3 °C/min under a 6 T field is shown in Fig. 1b. The primary peak at q^*=0.066 nm^{-1} corresponds to the lamellar period of $2\pi/q^*$=9.5 nm and T_{odt}=257 °C. The ordering transition takes place over an unusually broad temperature window spanning ≈8 °C, though the reasons for this breadth are unknown (Supplemental Material [16]). 2-D SAXS data at select temperatures show the initial non-aligned state at room temperature, the high temperature disordered state where only correlation hole scattering is visible, and finally the aligned state produced on cooling. To the best of our ability to measure it, ± 0.5 °C, T_{odt} is unaffected by the field application. The data indicate that the lamellae are aligned with their surface normals perpendicular to the field, a degenerate configuration, indicating $\Delta\chi < 0$, Fig. 1c. TEM views along and perpendicular to the field, Fig. 2, confirm the alignment of the microstructure and its degenerate nature.

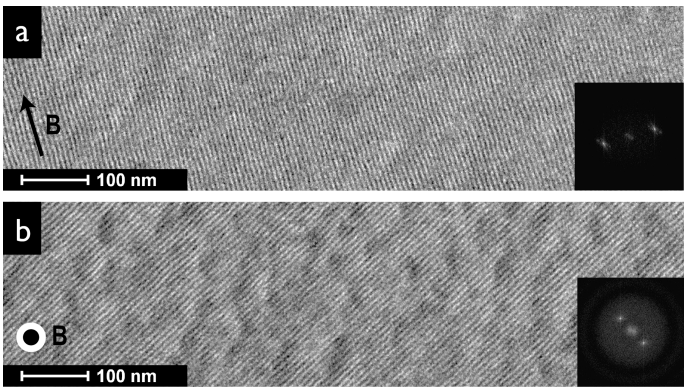

FIG. 2. TEM images and associated fast Fourier transforms (FFTs) of PS-b-P4VP aligned at 6 T visualized (a) perpendicular to the field direction and, (b) along the field direction.

Fig. 3a. shows SAXS data during cooling across T_{odt}. The evolution of order and alignment are visible in the gradual disappearance of the diffuse azimuthally uniform intensity due to correlation hole scattering, and the concurrent emergence of Bragg scattering concentrated in arcs centered on the equatorial line. The azimuthal dependence of the scattered intensity in the Bragg peak, $I(\varphi)$, reflects the orientation distribution of the lamellar normals in the plane of the diffractogram. The full width at half maximum (FWHM) of $I(\varphi)$ depends both on the cooling rate and the field strength, with the best alignment observed for the combination of smallest cooling rate, 0.1 °C/min, and largest field, 6 T, Fig. 3b-d.

The high degree of alignment suggests that the system has $\Delta\chi$ well in excess of the expected $\mathcal{O}(10^{-10})$ value. Experiments conducted with the secondary sample recovered similar results, dispelling any concerns regarding sample purity. Lamellar BCPs are known to form anisotropic, ellipsoidal, grains during nucleation and growth, with faster growth along the lamellar normal due to interfacial tension [19, 20]. Magnetic shape anisotropy for such grains is of a trivial magnitude as the suspending fluid is a disordered melt of identical composition to the grain. Further, even if dominant, shape anisotropy would align the ellipsoidal long axis parallel to the field [17], whereas here the observed alignment is orthogonal (Supplemental Material [16]).

The origin of the anisotropy can be understood partly by recognizing that real Gaussian chains are anisotropic entities as they possess finite end-end distances. Polarizability anisotropy has been treated in the context of

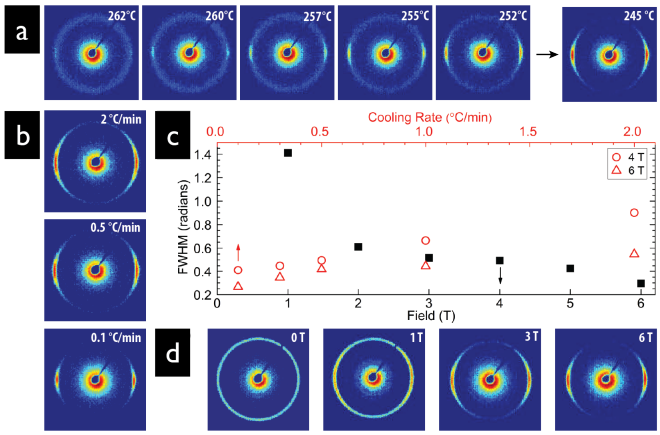

FIG. 3. (a) 2-D SAXS data at selected temperatures showing the emergence of aligned lamellae during cooling from the isotropic, disordered state at 0.3 °C/min at 6 T. (b) Diffractograms for samples under 6 T at 245 °C after cooling across T_{odt} at different rates indicated. (c) Dependence of azimuthal FWHM on field strength (at 0.3 °C/min) and cooling rate (at 4 and 6 T), on bottom and top x axes respectively. (d) Diffractograms at 245 °C after cooling across T_{odt} at 0.3 °C/min at indicated field strengths.

freely jointed statistical segments by Kuhn [21] yielding $\Delta\gamma = \gamma_1 - \gamma_2 = \frac{3}{5}(\alpha_1 - \alpha_2)R^2/\langle R^2\rangle_0$ where α_1 and α_2 are the polarizabilities parallel and perpendicular to the bonds joining statistical segments, R^2 is the squared end-end chain distance, and $\langle R^2\rangle_0$ is the unperturbed mean-squared end-end distance. The problem has also been treated in the context of the worm-like chain model by Benoit, Weill, *et al.* [22, 23]. While individual chains are anisotropic, the orientation of the end-end vectors in a melt are uncorrelated so there is no net anisotropy. The situation is different however for polymer brushes where one chain end is tethered to an impenetrable surface. This geometrically imposes a net anisotropy in which the orientation distribution of end-end vectors has its maximum along the surface normal, and in which the width of the distribution narrows with increasing areal density of the chains. The physical analogy between surface attachment of chain ends for a brush, and chain end (junction) localization at a BCP block interface provides a segue into treating chain anisotropy in BCPs. Indeed, the optical anisotropy of tethered chains has been considered in detail by Lodge and Fredrickson, for BCP melts [24]. They note the significance of intrinsic anisotropy relative to form anisotropy in the birefringence of lamellar mesophases and highlight the importance of orientational correlation of end-end vectors relative to chain stretching in dictating the intrinsic anisotropy.

Optical anisotropies have been investigated experimentally by depolarized Rayleigh scattering [25–27] and numerically based on bond polarizability data using the rotational isomeric states approaches advanced by Nagai [28], and by Flory and co-workers [26]. The statistical segment polarizability anisotropy $\Delta\alpha = \alpha_1 - \alpha_2$ cannot be linked readily to chemical structure as it is a quantity associated with a hypothetical construct, i.e. the statistical segment of the freely jointed model. $\Delta\alpha$ has been measured however for some polymers using stress-optical coefficients [21, 29]. These data are complemented by studies of electric field induced birefringence, the Kerr effect, in polymer solutions [30, 31]. The magnetic analog in the Cotton-Mouton coefficient for magnetic birefringence provides access to the chain magnetic susceptibility anisotropy as $C_m = (\Delta n/cB^2) \sim \Delta\chi\Delta\gamma$, with $\Delta\chi$ interpreted again in the context of the chain statistical element [32, 33]. Precise measurements of magnetic birefringence and segmental susceptibility anisotropy of chains in the melt are challenging, and there is little reported data that can be used in the present context.

In lieu of robust experimental data, we use MD to estimate $\Delta\chi$ for PS chains tethered at an impenetrable surface. We investigate the orientational order of backbone bonds and the side bonds to the phenyl ring as a function of degree of polymerization, N_p, and the chain areal density at the surface, σ, Fig. 4. The height of the brush scales as $H \sim N_p\sigma^{1/2}$, as expected for melt chains [34]. The orientational order with respect to the surface normal, the y-axis in Fig. 4a, for backbone and side bonds to the phenyl ring, $\langle P_2^b(\cos\varphi)\rangle$ and $\langle P_2^s(\cos\varphi)\rangle$ respectively, increase slowly, but approximately linearly with σ. There is no statistically significant MW dependence as expected for brushes where chain anisotropy is independent of N_p [24]. $\langle P_2^b\rangle$ and $\langle P_2^s\rangle$ differ in sign, reflecting the tendency of the backbone bonds, and therefore $\overrightarrow{R}$, to lie parallel to the surface normal, and the side bonds to be orthogonal to the backbone.

The areal density of chains at the block interface is $\sigma = \rho L_0 N_A/MW$ where L_0 is the lamellar period. Here, $\sigma \approx 1$ nm^{-2} which corresponds to $\sigma = 0.033$ in simulation units. The orientational order of the phenyl ring defined by the ring normal, $\langle P_2^p(\cos\varphi)\rangle$, is also calculated (Supplemental Material [16]). At this density, $\langle P_2^b(\cos\varphi)\rangle \approx 0.07$ and $\langle P_2^p(\cos\varphi)\rangle \approx 0.04$. We estimate $\Delta\chi$ based on the volume fraction, ϕ, weighted anisotropies of the alkane backbone ($\Delta\chi^b$) [35] and that of the phenyl ring ($\Delta\chi^p$) [15]. For the PS chains, $\Delta\chi = \phi^b\langle P_2^b(\cos\varphi)\rangle\Delta\chi^b + \phi^p\langle P_2^p(\cos\varphi)\rangle\Delta\chi^p \approx -1.6\times10^{-8}$. We expect a similar contribution from the P4VP block given the near identical susceptibilities of pyridine and benzene, and so for the system overall $\Delta\chi \approx -1.6\times10^{-8}$. Note that σ in BCPs is not arbitrarily determined as it is for brushes, but is a function of N_p and the Flory interaction parameter, χ (Supplemental Material [16]).

We use the estimated $\Delta\chi$ to consider the alignment data of Fig. 3. The azimuthal intensity dependence $I(\varphi)$ reflects the probability of observing lamellar normals at a given angle φ with respect to the field direction. This

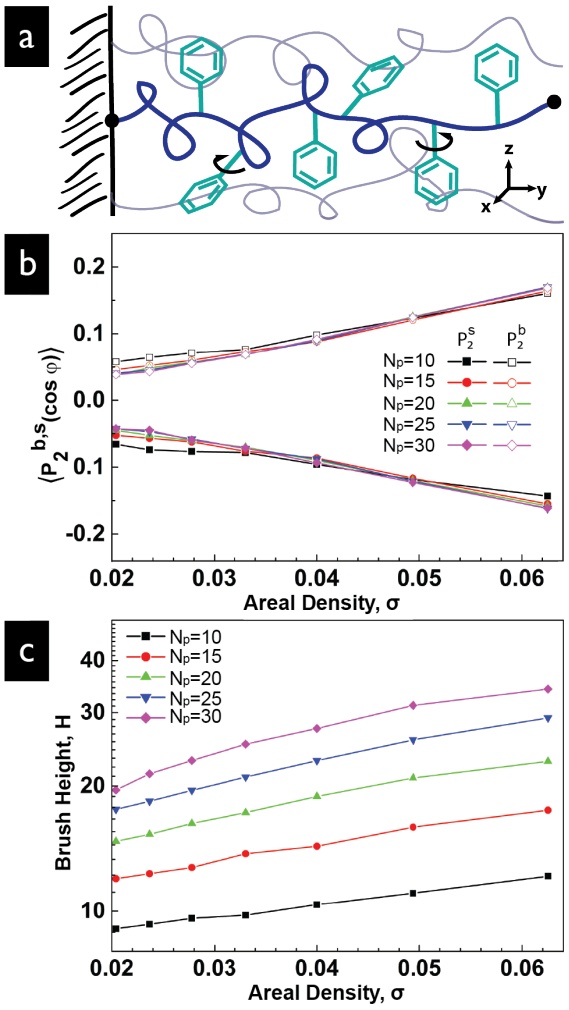

FIG. 4. (a) Illustration of a polystyrene chain tethered at an impenetrable surface. The phenyl rings can rotate around the side-bond to the backbone. (b) Simulated backbone, $\langle P_2^b\rangle$, and side chain, $\langle P_2^s\rangle$, orientation distribution coefficients as functions of areal density σ for varying N_p. (c) Simulated brush height, $H(\sigma)$, for varying N_p.

probability $p(\varphi, B)$, is governed by a Boltzmann factor incorporating the angle-dependent magnetostatic energy, $E_m(\varphi, B) = -(B^2/2\mu_0)\Delta\chi\xi^3\cos^2\varphi$, for a characteristic grain size, ξ, Eq. 3. The orientation distribution coefficient $\langle P_2\rangle$ resulting from $p(\varphi, B)$ may be evaluated by integration, Eq. 4. The orientation distribution coefficients are obtained as a function of field strength from Gaussian fits of the SAXS intensity profiles. We estimate the representative grain size by fitting the experimentally determined $\langle P_2\rangle$ to those calculated using Eq. 4, yielding $\xi \approx 1.2$ μm. This corresponds to a field interaction $\Delta E_m > 10^2$ kT. The results are shown in Fig. 5, with calculated field dependent P_2 for different grain sizes. It is important to note that the estimated grain size only provides the characteristic dimensions of a structural unit which would, at steady state, reproduce

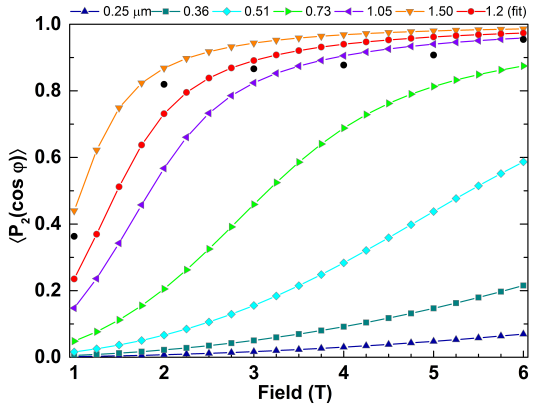

FIG. 5. Field-dependent orientation distribution coefficients (Eq. 4) for various grain sizes, ξ, for $\Delta\chi = -1.6 \times 10^{-8}$ at 245 °C. Black circles show experimentally derived values for samples cooled 0.3 °C/min. Fitting Eq. 4 (red circle trace) to experimental data yields $\xi \approx 1.2$ μm.

the orientation distribution measured in the aligned samples - larger grains subjected to kinetic hindrances could conceivably display the same orientation distribution as smaller grains in steady state. It is clear from the cooling rate dependence shown in Figure 3 that kinetic effects are present. Such kinetic effects during the cooling ramp as derived principally from the temperature-dependent viscosity of the system, as well as any Ostwald ripening, do not factor into our analysis. For comparison, assuming no contribution from chain anisotropy (i.e. with only domain anisotropy of $\Delta\chi = 1 \times 10^{-10}$), the observed alignment would imply the existence of uncharacteristically large grains of $\xi \approx 6.6$ μm at the elevated temperatures in close proximity to T_{odt} where alignment takes place. The actual grain sizes observed at room temperature would likely be significantly larger due to the aforementioned kinetic and ripening effects. This supports our assertion that domain anisotropy alone is insufficient to explain the observed data. Finally we note in passing that the greater uncertainty in determining P_2 at low vs. high field strengths (~1-2 T) likely contributes to the weaker agreement between the data and the fit at low fields.

$$p(\varphi, B) = \frac{e^{-E_m/kT}\sin\varphi\, d\varphi}{\int_0^\pi e^{-E_m/kT}\sin\varphi\, d\varphi} \tag{3}$$

$$\langle P_2(\cos\varphi)\rangle = \frac{\int_0^\pi \frac{1}{2}(3\cos^2\varphi - 1)\, e^{-E_m/kT}\sin\varphi\, d\varphi}{\int_0^\pi e^{-E_m/kT}\sin\varphi\, d\varphi} \tag{4}$$

The grain size determined by fitting is in modest agreement with an estimated size of ≈ 3 μm from sampling TEM images of field aligned samples. To provide better quantification we independently measured the grain size using a recently developed 'variance scattering' technique [18]. This approach statistically analyses the az-

imuthal intensity variation of a primary Bragg peak, from which the number of independent scatterers, and thus the grain size, can be quantified. On this basis we estimate $\xi \approx 5 - 6\,\mu$m at room temperature (Supplemental Material [16]). The fact that TEM and scattering derived grain sizes exceed the estimate based on the orientation distribution reflects the occurrence of microstructure coarsening without accompanying improvement in the alignment under the field. We should therefore view the estimated ξ as an upper bound for the characteristic grain size that pertained during the period in which the system was responsive to the field.

BCP nucleation and growth kinetics have been explored experimentally and theoretically with some success [19, 36–39]. The slow dynamics of high MW BCPs has largely restricted work to unentangled melts and concentrated solutions as a matter of convenience where grain sizes of $\sim 0.5 - 5$ μm are not uncommon. One can therefore expect that sufficiently large grains can be prepared in a variety of BCPs to enable alignment using magnetic fields. The slow dynamics of entangled melts and the inaccessibility of the ODT in high MW systems suggest that this strategy would be limited to melts below entanglement MW and concentrated solutions. It is clear that the aromatic nature of PS-b-P4VP contributes to a markedly larger $\Delta\chi$ than one would encounter for other common but non-aromatic polymers such as polyethylene oxide or polymethylmethacrylate. The fact however that $E_m \sim \xi^3$ means that for the purposes of alignment, an order of magnitude decrease in $\Delta\chi$ can be compensated for by an increase in ξ by a factor of just over 2.

This work was supported by NSF under DMR-1119826 and DMR-1410568. Facilities use was supported by YINQE. Additionally, this research used resources of the Center for Functional Nanomaterials, which is a U.S. DOE Office of Science Facility, at Brookhaven National Laboratory under Contract No. DE-SC0012704. The authors thank Nitash Balsara and Zhen-Gang Wang for fruitful discussions, and Mike Degen (Rigaku Inc.) and AMI Inc. for technical support.

[1] S. Darling, Prog. Polym. Sci. **32**, 1152 (2007).
[2] H. Hu, M. Gopinadhan, and C. O. Osuji, Soft Matter **10**, 3867 (2014).
[3] A. Böker, H. Elbs, H. Hänsel, A. Knoll, S. Ludwigs, H. Zettl, V. Urban, V. Abetz, A. H. E. Müller, and G. Krausch, Phys. Rev. Lett. **89**, 135502 (2002).
[4] T. Xu, Y. Zhu, S. P. Gido, , and T. P. Russell, Macromolecules **37**, 2625 (2004).
[5] C. Liedel, C. W. Pester, M. Ruppel, V. S. Urban, and A. Böker, Macromol. Chem. Phys. **213**, 259 (2012).
[6] P. W. Majewski, M. Gopinadhan, and C. O. Osuji, Journal of Polymer Science Part B: Polymer Physics **50**, 2 (2012).
[7] C. Osuji, P. J. Ferreira, G. Mao, C. K. Ober, J. B. Vander Sande, and E. L. Thomas, Macromolecules **37**, 9903 (2004).
[8] Y. Tao, H. Zohar, B. D. Olsen, and R. A. Segalman, Nano Lett. **7**, 2742 (2007).
[9] M. Gopinadhan, P. W. Majewski, Y. Choo, and C. O. Osuji, Phys. Rev. Lett. **110**, 078301 (2013).
[10] P. Deshmukh, M. Gopinadhan, Y. Choo, S.-k. Ahn, P. W. Majewski, S. Y. Yoon, O. Bakajin, M. Elimelech, C. O. Osuji, and R. M. Kasi, ACS Macro Lett. **3**, 462 (2014).
[11] T. Grigorova, S. Pispas, N. Hadjichristidis, and T. Thurn-Albrecht, Macromolecules **38**, 7430 (2005).
[12] A. Buka and W. De Jeu, J. Phys. **43**, 361 (1982).
[13] J. Bunning, D. Crellin, and T. Faber, Liq. Cryst. **1**, 37 (1986).
[14] P. Sotta, S. Valić, B. Deloche, D. Maring, and H. W. Spiess, Acta Polymerica **50**, 205 (1999).
[15] M. Kumar, *Diamagnetic Susceptibility and Magnetic Anisotropy of Organic Compounds* (Springer, 2008).
[16] See Supplemental Material at [url] for details of experimental methods, MD simulations, shape anisotropy considerations and grain size calculations, which includes Refs. [17, 18].
[17] J. F. Schenck, Med. Phys. **23**, 815 (1996).
[18] K. G. Yager and P. W. Majewski, J. Appl. Crystallogr. **47**, 1855 (2014).
[19] T. Hashimoto, N. Sakamoto, and T. Koga, Phys. Rev. E **54**, 5832 (1996).
[20] N. P. Balsara, C. M. Marques, B. A. Garetz, M. C. Newstein, and S. P. Gido, Phys. Rev. E **66**, 052802 (2002).
[21] W. Kuhn and F. Grun, Kolloid-Z. **101**, 248 (1942).
[22] M. Arpin, C. Strazielle, G. Weill, and H. Benoit, Polymer **18**, 262 (1977).
[23] G. Maret and G. Weill, Biopolymers **22**, 2727 (1983).
[24] T. P. Lodge and G. H. Fredrickson, Macromolecules **25**, 5643 (1992).
[25] A. Tonelli, Y. Abe, and P. Flory, Macromolecules **3**, 303 (1970).
[26] U. W. Suter and P. J. Flory, J. Chem. Soc., Faraday Trans. **73**, 1521 (1977).
[27] G. Fytas, A. Patkowski, G. Meier, and E. Fischer, Macromolecules **21**, 3250 (1988).
[28] K. Nagai, J. Chem. Phys. **40**, 2818 (1964).
[29] R. Stein and A. Tobolsky, J. Polym. Sci. **11**, 285 (1953).
[30] J. Champion, in *Developments in Polymer Characterisation* (Springer, 1980), pp. 207–237.
[31] V. Tsvetkov, L. Andreeva, and N. Tsvetkov, Wiley Database of Polymer Properties (1989).
[32] G. Maret and K. Dransfeld, Top. Appl. Phys. **57**, 143 (1985).
[33] U. Tiesler, M. Rehahn, M. Ballauff, G. Petekidis, D. Vlassopoulos, G. Maret, and H. Kramer, Macromolecules **29**, 6832 (1996).
[34] S. Milner, T. Witten, and M. Cates, Macromolecules **21**, 2610 (1988).
[35] H. H. Shao, H. Gang, and E. B. Sirota, Phys. Rev. E **57**, R6265 (1998).
[36] G. H. Fredrickson and K. Binder, J. Chem. Phys. **91**, 7265 (1989).
[37] H. J. Dai, N. P. Balsara, B. A. Garetz, and M. C. Newstein, Phys. Rev. Lett. **77**, 3677 (1996).
[38] J. Goveas and S. Milner, Macromolecules **30**, 2605 (1997).
[39] T. Q. Chastek and T. P. Lodge, Macromolecules **37**, 4891 (2004).